AFRL-RW-EG-TP-2012-002

Effects of Processing and Powder Size on Microstructure and Reactivity in Arrested Reactive Milled Al + Ni

Eric B. Herbold[2]
Jennifer L. Jordan[1]
N.N. Thadhani[2]

[1]Air Force Research Laboratory, AFRL/RW, Eglin AFB, FL 32542

[2]School of Materials Science and Engineering, Georgia Institute of Engineering, Atlanta, GA 30332

May 2012

Interim Report

AIR FORCE RESEARCH LABORATORY, MUNITIONS DIRECTORATE

Air Force Materiel Command ■ United States Air Force ■ Eglin Air Force Base

NOTICE AND SIGNATURE PAGE

Using Government drawings, specifications, or other data included in this document for any purpose other than Government procurement does not in any way obligate the U.S. Government. The fact that the Government formulated or supplied the drawings, specifications, or other data does not license the holder or any other person or corporation; or convey any rights or permission to manufacture, use, or sell any patented invention that may relate to them.

Qualified requestors may obtain copies of this report from the Defense Technical Information Center (DTIC) (http://www.dtic.mil).

AFRL-RW-EG-TP-2012-002 HAS BEEN REVIEWED AND IS APPROVED FOR PUBLICATION IN ACCORDANCE WITH ASSIGNED DISTRIBUTION STATEMENT.

FOR THE DIRECTOR:

WHITE.HOWARD.G.1230779062 Digitally signed by WHITE.HOWARD.G.1230779062 DN: c=US, o=U.S. Government, ou=DoD, ou=PKI, ou=USAF, cn=WHITE.HOWARD.G.1230779062 Date: 2012.05.08 10:12:31 -05'00'

HOWARD G. WHITE, PhD
Technical Advisor
Ordnance Division

VARNER.CHRISTOPHER.L.1265664543 Digitally signed by VARNER.CHRISTOPHER.L.1265664543 DN: c=US, o=U.S. Government, ou=DoD, ou=PKI, ou=USAF, cn=VARNER.CHRISTOPHER.L.1265664543 Date: 2012.05.02 06:52:29 -05'00'

CHRISTOPHER L. VARNER
Branch Chief
Energetic Materials Branch

JORDAN.JENNIFER.L.1265297915 Digitally signed by JORDAN.JENNIFER.L.1265297915 DN: c=US, o=U.S. Government, ou=DoD, ou=PKI, ou=USAF, cn=JORDAN.JENNIFER.L.1265297915 Date: 2012.05.08 07:41:58 -05'00'

JENNIFER L. JORDAN, PhD
Project Manager
Energetic Materials Branch

This report is published in the interest of scientific and technical information exchange, and its publication does not constitute the Government's approval or disapproval of its ideas or findings.

This page intentionally left blank

REPORT DOCUMENTATION PAGE

Form Approved
OMB No. 0704-0188

1. REPORT DATE *(DD-MM-YYYY)*	**2. REPORT TYPE**	**3. DATES COVERED** *(From - To)*
05-2012	Interim	October 2009 – February 2011

4. TITLE AND SUBTITLE

Effects of Processing and Powder Size on Microstructure and Reactivity in Arrested Reactive Milled Al + Ni

5a. CONTRACT NUMBER

5b. GRANT NUMBER

5c. PROGRAM ELEMENT NUMBER
62102F

6. AUTHOR(S)

Eric B. Herbold[2], Jennifer L. Jordan[1], N.N. Thadhani[2]

5d. PROJECT NUMBER
4347

5e. TASK NUMBER
95

5f. WORK UNIT NUMBER
05

7. PERFORMING ORGANIZATION NAME(S) AND ADDRESS(ES)

[1]Air Force Research Laboratory, AFRL/RW, Eglin AFB, FL 32542
[2]School of Materials Science and Engineering, Georgia Institute of Engineering, Atlanta, GA 30332

8. PERFORMING ORGANIZATION REPORT NUMBER

AFRL-RW-EG-TP-2012-002

9. SPONSORING / MONITORING AGENCY NAME(S) AND ADDRESS(ES)

Air Force Research Laboratory, Munitions Directorate
Ordnance Division
Energetic Materials Branch (AFRL/RWME)
Eglin AFB FL 32542-5910
Technical Advisor: Dr. Jennifer L. Jordan

10. SPONSOR/MONITOR'S ACRONYM(S)
AFRL-RW-EG

11. SPONSOR/MONITOR'S REPORT NUMBER(S)
AFRL-RW-EG-TP-2012-002

12. DISTRIBUTION / AVAILABILITY STATEMENT

Distribution A: Approved for public release; distribution unlimited. Approval Confirmation 96 ABW/PA # 96ABW-2011-003, dated January 14, 2011

13. SUPPLEMENTARY NOTES

DISTRIBUTION STATEMENT INDICATING AUTHORIZED ACCESS IS ON THE COVER PAGE AND BLOCK 12 OF THIS FORM.

14. ABSTRACT

Ball-milling Al-metal powders can result in self-sustaining high-temperature synthesis in intermetallic-forming systems. Here, Al and Ni powders with similar composition are used to investigate how microstructural differences affect the measured time to reaction (TTR) between powders of different sizes processed under milling conditions specified by statistically designed experiments. Linear statistical models predicting the TTR and the change in temperature (DT) are built from these experimental results. The time required to observe a self-sustained high-temperature synthesis of NiAl with different combinations of the powders and ball-milling conditions vary by almost an order of magnitude. Comparisons of powders milled to times corresponding to percentages of their averaged TTR show similar reaction initiation temperatures despite the difference in total milling time. Several distinct arrested reactions within the powder grains exhibit rapid solidification or incomplete diffusion of Ni into Al, forming porous Ni-rich layered structures. The partially reacted grains suggest that the composite laminate particles are not forming intermetallic on the grain scale, but on the localized scale between layers.

15. SUBJECT TERMS

High-energy ball-milling; Self-propagating high-temperature synthesis; Differential scanning calorimetry; X-ray diffraction

16. SECURITY CLASSIFICATION OF:			**17. LIMITATION OF ABSTRACT**	**18. NUMBER OF PAGES**	**19a. NAME OF RESPONSIBLE PERSON**
a. REPORT	**b. ABSTRACT**	**c. THIS PAGE**			Jennifer L. Jordan
UNCLASSIFIED	UNCLASSIFIED	UNCLASSIFIED	UL	19	**19b. TELEPHONE NUMBER** *(include area code)* 850-882-8992

Standard Form 298 (Rev. 8-98)
Prescribed by ANSI Std. Z39.18

This page intentionally left blank

Available online at www.sciencedirect.com
ScienceDirect
Acta Materialia xxx (2011) xxx–xxx
Acta MATERIALIA
www.elsevier.com/locate/actamat

Effects of processing and powder size on microstructure and reactivity in arrested reactive milled Al + Ni

E.B. Herbold [a,b,*], J.L. Jordan [a], N.N. Thadhani [b]

[a] High Explosives Research and Development Branch, Munitions Directorate, Air Force Research Laboratory, Eglin AFB, FL 32542, USA
[b] School of Materials Science and Engineering, Georgia Institute of Technology, Love Manufacturing Building, 771 Ferst Drive, Atlanta, GA 30332, USA

Received 8 February 2011; received in revised form 14 June 2011; accepted 13 July 2011

Abstract

Ball-milling Al-metal powders can result in self-sustaining high-temperature synthesis in intermetallic-forming systems. Here, Al and Ni powders with similar composition are used to investigate how microstructural differences affect the measured time to reaction (TTR) between powders of different sizes processed under milling conditions specified by statistically designed experiments. Linear statistical models predicting the TTR and the change in temperature (ΔT) are built from these experimental results. The time required to observe a self-sustained high-temperature synthesis of NiAl with different combinations of the powders and ball-milling conditions vary by almost an order of magnitude. Comparisons of powders milled to times corresponding to percentages of their averaged TTR show similar reaction initiation temperatures despite the difference in total milling time. Several distinct arrested reactions within the powder grains exhibit rapid solidification or incomplete diffusion of Ni into Al, forming porous Ni-rich layered structures. The partially reacted grains suggest that the composite laminate particles are not forming intermetallic on the grain scale, but on the localized scale between layers.
Published by Elsevier Ltd. on behalf of Acta Materialia Inc.

Keywords: High-energy ball-milling; Self-propagating high-temperature synthesis; Differential scanning calorimetry; X-ray diffraction

1. Introduction

High energy ball-milling has been used extensively to intimately mix metal–metal or metal–metal-oxide powders. The powder is processed through repeated impacts of a "grinding" media usually made from elastically deforming spherical balls enclosed in a sealed container; this processing produces materials with highly refined microstructures, enhanced strength or metastable phases [1–16]. This technique has been shown to synthesize intermetallic compounds resulting from gradual and explosive formation at the grain level [3,4,6,9–13]. A self-sustained high-temperature synthesis (SHS) of intermetallics may release large amounts of heat during intermetallic phase formation on the order of that released by explosives [17]. The gasless reaction from reactive milled (RM) experiments forming nickel aluminides [3,4,6,8–10,12,15,16,18,19], titanium-based alloys [5] and combustion reactions in metal–metal-oxides [11,13,14] in a ball-mill are several examples of materials that exhibit SHS.

The microstructure within ball-milled powder grains is highly heterogeneous and is refined during processing until reaction occurs. The refinement process consists of the cold welding of powder grains within the contact areas where balls either impact with one another or with the walls of the vessel [5,8,21]. Prior to reaction, the particle microstructure may consist of many layers due to the flattening of the particles for materials of relatively high deformability. Many investigations have been reported on the kinetics of reaction in idealized multilayered intermetallic systems that may be applicable to the reactions observed

* Corresponding author. Present address: Computational Geosciences Group, Lawrence Livermore National Laboratory, Livermore, CA 94550, USA. Tel.: +1 925 422 1659; fax: +1 925 423 3886.
E-mail address: herbold1@llnl.gov (E.B. Herbold).

1359-6454/$36.00 Published by Elsevier Ltd. on behalf of Acta Materialia Inc.
doi:10.1016/j.actamat.2011.07.029

in ball-milled powder particles [17–19,22,24,25]. It was shown in Ref. [17] that reaction propagation velocities in sputter-deposited Al/Ni and Al/Monel are affected by the layer thickness, temperature and intermixing at the material interface. Additionally, the heat of reaction was found to be lower for laminate thicknesses less than 50 nm due to the amount of interfacial mixing [17]. Atomistic simulations of Al/Ni nanolaminates under shock loading have shown that the introduction of voids either at the interface of the layers or within the Al enhanced the rate of intermetallic reaction [26]. By comparison, prerequisite conditions for reaction in Al/Ni powders observed in high-energy ball-milling are a suitable reduction in the layer thickness, and it has been suggested that solid-state diffusion times are decreased by several orders of magnitude as defect densities increase [8,27].

Recent investigations show that arrested reactive milling (ARM) techniques can be used to ball-mill constituent powders to a point where they are well blended but have not reacted; this constitutes an important class of candidate materials for heat sources in joining applications [17] or additions to explosive materials [20,28–31]. The layers within the particles may exhibit a very high defect density depending on the impact energy of the grinding media against the vessel walls and the deformability of the constituent powders, which changes with each subsequent impact.

In our recent work, it was shown that the reaction initiation threshold in mixed and ball-milled Ni + Al powders[1] under high-rate mechanical loading depends on the microstructure within the powder particles and the level of strain-hardening, which change as a function of processing time [18]. Comparisons between mixed and ball-milled powders showed a reduction in the mechanically induced reaction initiation for moderate milling times that is attributed, in part, to the high specific surface area between constituent materials. However, upon further milling and corresponding reduction in layer thickness within the powder grains, the reduced ductility resulted in a higher mechanically activated reaction initiation threshold. Thus, the optimum amount of ball-milling was found to depend on the grain microstructure and the level of strain hardening. This dependence is sensitive to the ball-milling process variables, which is addressed in this investigation.

Here we investigate high-energy ball-milling of nominally spherical Ni and Al powders in an equiatomic ratio and vary particle sizes and ball-milling conditions to compare the microstructural differences and reaction characteristics of ARM materials. The time required to observe SHS with different combinations of the powders and ball-milling conditions shown here vary by almost an order of magnitude.[2] Here the time to reaction (TTR) is used as a basis for comparison between the powders, which will be useful in both thermal and X-ray analysis. Three materials are selected to determine the average TTR for given particle sizes and milling conditions to compare the powders as a function of milling time needed for SHS. The temperature change on the outside of the vessel containing the powder is also measured and used to indicate the specific energy release during alloy formation. The resulting NiAl powder grains show signs of melting and void creation, as expected, and several partially reacted powder grains are shown and discussed.

2. Experimental methods

2.1. Ball-milling

For each ball-milling operation, the powders, stainless steel grinding media and process control agent (PCA) were loaded and unloaded into a stainless steel vial within a glovebox filled with Ar. Although Ar has been shown to increase the ambient temperature within the vial, it is used to prevent nitride or oxide formation (see Chapter 15 in Ref. [27]). Four stainless steel vials were used at random to reduce the dependence of milling on any contaminant deposits or difference in roughness on the inside surfaces. It is shown in Ref. [32] that contamination is an order of magnitude less when using stainless steel vials and grinding media: 0.35% Fe contamination was reported for 8 h of continuous milling [21]. Each ball-milling experiment is performed with a molar ratio of $Ni_{0.5}Al_{0.5}$ with three different Ni powders (Ni: 5–15 μm, −300 mesh, −150 + 200, 99.8% pure, Alfa Aesar) and Al powders (Al: H2, H30, H50, 99.7% pure, Valimet, Inc.). The powder was milled in a SPEX-8000 shaker mill (SPEX CertiPrep® Group) with varying amounts of stearic acid as a percentage of the total powder mass (95% reagent grade, Sigma Aldrich) [5]. A recent investigation shows that varying the milling intensity by grinding powders with media of different density affects the degree of refinement and subsequent reaction [14]. Here, changing the size of the milling media varies the milling intensity. Fresh grinding media is used for each experiment to aid in the reduction of Fe contamination due to surface deterioration [8,27].

In total, seven variables are considered: the diameter of the grinding media (d_b (mm)), the charge ratio (i.e. mass of grinding media to the mass of powder, r_{bp}), the total powder mass (m_p (g)), the controlled temperature (T_c (°C)), the size of the Ni and Al powders (d_{Ni} and d_{Al} (μm)), and the amount of PCA (m_{PCA}/m_p). Testing each variable at two different levels would require 128 experiments to quantify the individual or combined effects these changes have on the measured TTR and the temperature change of the vial. Design and analysis experiments principles were used to systematically reduce the number of experiments while maintaining as much information as possible for quantitative analysis [33]. These principles allow us to quantify our results while changing more than one variable at a time (i.e. a factorial design). The term "designed experiments" is

[1] The powders investigated in Ref. [18] are identical to those discussed herein.

[2] This is shown in Table 2 by comparing the time to reaction values from Experiments 10 and 17.

Please cite this article in press as: Herbold EB et al. Effects of processing and powder size on microstructure and reactivity in arrested reactive milled Al + Ni. Acta Mater (2011), doi:10.1016/j.actamat.2011.07.029

Table 1
Experimental plan for milling 1:1 Ni + Al powders. Experiments 17–39 are part of the designed experiments. The PCA was stearic acid ($C_{18}H_{36}O_2$) and was added as a percentage of the total powder mass.

Experiment no.	Ball diameter (mm)	Charge ratio	Powder mass (g)	Controlled temperature (°C)	Al (μm)	Ni (mesh (μm))	% PCA* (%)
10	5.56	10	10	32	50	−150 + 200	1
17	7.94	2.5	20	32	50	−150 + 200	1
18	3.18	5.5	20	32	50	[5–15]	7
19	7.94	5.5	20	32	2	[5–15]	1
22	5.56	4.0	15	27	30	−300	4
21	3.18	2.5	20	21	2	[5–15]	1
23	3.18	5.5	10	21	2	[5–15]	7
24	7.94	2.5	20	21	50	[5–15]	7
25	3.18	2.5	10	21	50	−150 + 200	7
26	7.94	2.5	10	32	2	[5–15]	7
27	5.56	4.0	15	27	30	−300	4
28	7.94	5.5	10	32	50	−150 + 200	7
29, 43, 46, 50, 51, 57, 58	7.94	5.5	10	21	50	[5–15]	1
30	3.18	5.5	20	21	50	−150 + 200	1
31	5.56	4.0	15	27	30	−300	4
32, 44, 47, 52, 53, 59, 60	7.94	2.5	10	21	2	−150 + 200	1
33	3.18	2.5	10	32	50	[5–15]	1
34	7.94	5.5	20	21	2	−150 + 200	7
35, 45, 48, 54, 55, 61, 62	3.18	5.5	10	32	2	−150 + 200	1
36	3.18	2.5	20	32	2	−150 + 200	7
39	5.56	4.0	15	27	30	−300	0.5

used in this paper to acknowledge use of a factorial design. A resolution 3 fractional factorial design of experiments (DOE) with replicated center points is shown in Table 1 where the reduction in the number of experiments is achieved at the expense of aliasing main effects with two-factor interactions. A full explanation of this design is beyond the scope of this paper, but can be found in Ref. [33]. Regression analysis of the factors affecting the TTR is performed with Design Expert software [34].

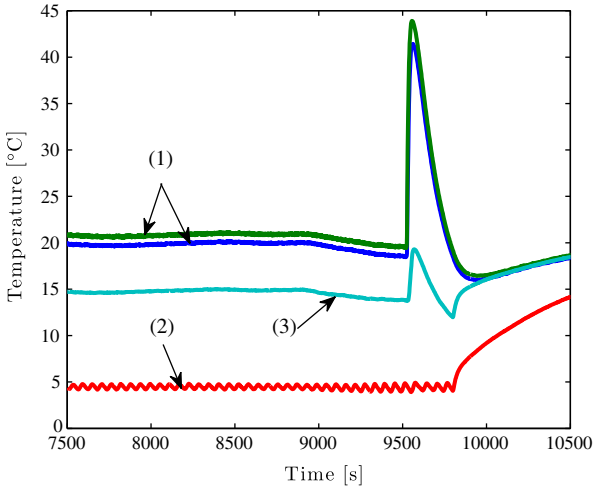

Fig. 1. Typical temperature measurements from the thermocouples during ball-milling taken from Experiment 29. The two curves marked by (1) are the temperature measured at the bottom (top curve) and top (bottom curve) of the cylindrical vial. The temperature profile of the coolant entering (curve (2)) and leaving (curve (3)) the cooling coil.

Two thermocouples (Omega, SA2F-K) with a USB-5201 data-logging device (Measurement Computing Corp.) are attached to a 1 mm thick Cu plate mounted between the bottom of the vial and the clamp for redundant temperature monitoring with a program written in LabView. The ball-mill is equipped with temperature control using a Cole-Parmer polystat chiller running ethylene glycol and water (1:1 volume ratio) through polyethylene tubing flowing through a custom Cu coil with 11 turns. The temperature is automatically adjusted via a servo-actuated valve to increase or decrease the flow of coolant. The mill motor is turned off automatically at the detection of a specified critical temperature, indicating reaction was achieved (see Fig. 1). A time limit was specified at 8 h such that the motor would cease operation if reaction had not occurred. In the event that the mill stopped for any reason other than a reaction before this time, the experiment was repeated to obtain a TTR from continuous milling.

2.2. Powder characterization

The particle morphology is visualized by scanning electron microscopy (SEM) using backscattered and secondary electron images from a JEOL JSM-5900LV microscope, and analyzed by energy dispersive spectrometry (EDS) (Oxford Link ISIS). The powders are embedded within an epoxy matrix and then polished to investigate the subgrain microstructure. The powder phase composition was deter-

Please cite this article in press as: Herbold EB et al. Effects of processing and powder size on microstructure and reactivity in arrested reactive milled Al + Ni. Acta Mater (2011), doi:10.1016/j.actamat.2011.07.029

mined using X-ray diffraction (XRD) results from a Philips X'Pert Pro MPD powder diffractometer operated at 50 kV and 20 mA with Cu K_α radiation at 1.5418 Å. Soller slits of 0.04 rad with a 10 mm mask were used to limit the axial divergence of the beam. Thermal characterization of the arrested reactive milled powders is performed with a Mettler-Toledo TGA/DSC STARe system at 20 K min^{-1} with 110 ml argon flowing over the furnace and a Al_2O_3 crucible.

3. Results

3.1. Ball-milling temperature measurements

The measured results from the designed experiments shown in Table 1 are listed in Table 2. The variation in the measured composition of powders is less than 1%, which should not prohibit the intermetallic reaction since it may take place above or below its stoichiometric ratio [9]. The measured mass of the grinding media and powders are given along with the temperature change, measured as the relative height of the temperature spike from the thermocouples shown by the peak with a height of 24 °C around 9500 s in Fig. 1 for Experiment 29. Table 2 shows that reactions occur within 8 h for PCA levels of 1% or lower. Higher levels of stearic acid reduce the level of cold welding at the surface of deforming particles, which promotes microstructural refinement, but increases the TTR at and above 4%. It has also been shown recently that increasing levels of PCA from 2% to 4% decreases the solubility of supersaturated Mg in Al by 5% at intermediate times of milling between 2 and 8 h [14].

In the second to last column of Table 2, the temperature change (ΔT) due to reaction ranges from 21 to 45 °C. This quantity is scaled by the mass of the powder and shown in Fig. 2 plotted as a function of the TTR. The value of ΔT is the difference between the maximum temperature and the controlled temperature (see the peak amplitude in Fig. 1). Each data point is labeled with its experimental number for comparison with Tables 1 and 2. The point sets marked with ○, □, or × indicate the repetition of experiments 29, 32 and 35, respectively. The ▽ marker indicates the remaining points. Assuming the specific heat is the same for all powders, this figure also indicates the variation in specific energy release detected during reaction, which is approximately 30%. It should be mentioned that reactions using 20 g of Ni and Al were observed within 8 h with charge ratios as low as 2.5 (see Experiment 17) and in the case of Experiment 19, the powder formed a melt pool within the vial, whereas all other reactions resulted in NiAl powder.

Table 2
Sample preparation measurements corresponding to the designed experiments presented in Table 1. Temperatures in parenthesis indicate the temperature change due to the intermetallic reaction during continuous ball-milling. The time to reaction indicates that many of the experiments were terminated at the specified 8 h time limit.

Experiment no.	Mass balls (g)	Mass Al (g)	Mass Ni (g)	Mass PCA (g)	Mean temperature (ΔT) (°C)	Time to reaction (s)
10	100	3.15	6.85	0.10	32 (23)	4740
17	49.98	6.299	13.702	0.200	32 (45)	25,416
19	109.6	6.299	13.702	0.201	32 (37)	15,588
22	60.28	4.718	10.261	0.592	27	>28,800
21	50.00	6.268	13.800	0.197	21	>28,800
23	55.00	3.138	6.812	0.707	21	>28,800
24	49.81	6.285	13.704	1.412	21	>28,800
25	25.00	3.142	6.844	0.702	21	>28,800
26	25.84	3.149	6.834	0.699	32	>28,800
27	60.28	4.719	10.331	0.594	27	>28,800
28	55.84	3.145	6.847	0.700	32	>28,800
29	55.91	3.145	6.854	0.103	21 (24)	9525
30	110.0	6.291	13.703	0.200	21 (37)	21,065
31	60.29	4.721	10.276	0.601	27	>28,800
32	25.93	3.156	6.849	0.098	21 (25)	11,696
33	25.00	3.147	6.846	0.105	32	>28,800
34	110.0	6.301	13.705	1.395	21	>28,800
35	54.97	3.146	6.855	0.106	32 (22)	12,708
36	50.02	6.297	13.702	1.399	32	>28,800
39	60.29	4.723	10.275	0.085	27 (28)	12,454
43	55.76	3.149	6.848	0.105	21 (22)	10,951
44	25.99	3.152	6.854	0.102	21 (23)	12,534
45	54.99	3.147	6.849	0.100	32 (21)	11,948
46	55.99	3.147	6.851	0.098	21 (21)	9412
47	25.907	3.149	6.849	0.109	21 (22)	13,665
48	54.991	3.152	6.849	0.100	32 (21)	11,946

3.2. Evolution of the powder microstructure

Experiments 29, 32 and 35 were selected to compare the microstructural differences due to varying particle and mill-

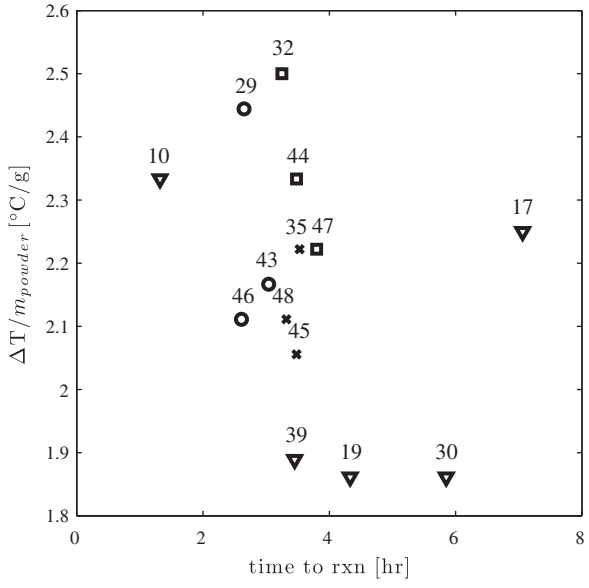

Fig. 2. The measured temperature change from reaction during milling is scaled by the mass of the powder and plotted as a function of the time to reaction. The value of ΔT is the difference between the maximum temperature and the controlled temperature (see the peak amplitude in Fig. 1). Each data point is labeled with its experimental number for comparison with Tables 1 and 2. The point sets marked with ○, □, or × indicate the repetition of Experiments 29, 32 and 35, respectively. The ▽ marker indicates the remaining points. Assuming the specific heat is the same for all powders, this figure also indicates the variation in specific energy release detected during reaction, which is approximately 30%.

Please cite this article in press as: Herbold EB et al. Effects of processing and powder size on microstructure and reactivity in arrested reactive milled Al + Ni. Acta Mater (2011), doi:10.1016/j.actamat.2011.07.029

ing media sizes and were repeated to determine the average TTR, which are listed in Table 3. Powders milled with these specific milling conditions and particle sizes are designated as ARM1 (data columns 1–3 in Table 3), ARM2 (columns 4–6) and ARM3 (columns 7–9). The TTR was reproducible within 10% and this average value is used in subsequent ARM experiments to quantify how long the powders have been processed with respect to the known milling time needed for reaction (e.g. ARM1–ARM3 powders were milled for 35% and 65% TTR). Subsequent ball-milling experiments were performed as a percentage of these average TTR values for microstructural evaluation, which is listed with the powder and milling media mass measurements in Table 4, and processing conditions in Table 1.

The initial Ni and Al powders are shown in Fig. 3a and b; the particles are nominally spherical and differ in size by about a factor of 10 times. Fig. 3c shows the microstructure of these powders milled under ARM1 conditions for 35% TTR. Based on the grayscale tone within the particle, small Ni (light gray) and Al particles (darker gray) can be differentiated within the composite powder particles. Void space is also apparent between the Ni and Al particles, which may be due to the resistance of the small Ni particles to deformation in comparison with larger particles. In Fig. 3d the microstructure is shown for identical powders milled under ARM1 conditions for 65% TTR. The composite particles are composed fine layers of Ni and Al and there are no signs of voids as in Fig. 3c. It is also apparent that the distribution of components is more uniform in comparison with Fig. 3c.

Fig. 4 shows the initial powder morphology and microstructural development of the powders milled under ARM2 conditions. In comparison with Fig. 3, the Ni particles are about 20 times larger and there are distinct surface asperities on surface of the larger particles in Fig. 4a. The Al particles in Fig. 4b are approximately 20 times smaller than those in Fig. 3a and were shipped in air. The smaller particles may introduce a higher Al_2O_3 contamination in the milled powders. In Fig. 4c the microstructure is shown after milling for 35% TTR. It appears that the large Ni particles were deformed much more than the 5 μm Ni particles shown in Fig. 3a, and their flattened shape resulted in composite particles without gaps between the constituents when comparing Figs. 4c and 3c. Despite the differences between Figs. 3 and 4 for a milling time of 35% TTR, the particle morphology is quite similar at 65% TTR when comparing Figs. 4d and 3d in terms of layer thickness. The major difference between the two powders (ARM1 and

Table 3
Experimental results for milling Ni + Al powders. Each column lists the milling parameters and measured results of the repeated experiments to determine the average time to reaction (TTR) and the standard deviation from this value.

Variable	Units	Results								
Experiment no.		29	43	46	32	44	47	35	45	48
Ball diameter	mm	7.94			7.94			3.18		
Charge ratio		5.5:1			2.5:1			5.5:1		
Al size[a]	μm	59			3.2			3.2		
Ni size[b]	μm	10			90			90		
Controlled Temperature	°C	21			21			32		
Time to reaction (TTR)	s	9525	10,951	9400	11,696	12,534	13,665	12,700	11,948	11,946
Average TTR	s	9959 (862)			12,632 (988)			12,198 (435)		
ΔT	°C	24	22	21	25	23	22	22	21	21

[a] Al particle sizes come from the H50 and H2 designation from Valimet (H50: 50 vol.% < 59 μm, 90 vol.% < 90 μm. H2: 50 vol.% < 3.2 μm, 90 vol.% < 6.8 μm).

[b] Ni particle sizes are averaged from the manufacturer's specifications (e.g. 10 and 90 μm are the average size of a distribution ranging from 5–15 μm and 74–105 μm, respectively.

Table 4
Milling measurements for ARM1–ARM3 powders. These powders were milled for a percentage of TTR values listed in Table 3.

Experiment no.	Mass balls (g)	Mass Al (g)	Mass Ni (g)	Mass PCA (g)	Mill Time (%TTR) (s)
50	56.75	3.146	6.849	0.101	3486 (35)
51	55.76	3.146	6.850	0.101	6480 (65)
52	25.91	3.148	6.851	0.990	4420 (35)
53	25.91	3.151	6.851	0.100	8210 (65)
54	54.99	3.149	6.850	0.101	4268 (35)
55	54.99	3.150	6.850	0.100	7920 (65)
57	55.90	3.148	6.846	0.098	3486 (35)
58	55.69	3.150	6.850	0.097	6472 (65)
59	25.91	3.150	6.852	0.098	4420 (35)
60	25.92	3.144	6.849	0.099	8210 (65)
61	54.99	3.151	6.856	0.100	4268 (35)
62	54.99	3.148	6.846	0.095	7928 (65)

Please cite this article in press as: Herbold EB et al. Effects of processing and powder size on microstructure and reactivity in arrested reactive milled Al + Ni. Acta Mater (2011), doi:10.1016/j.actamat.2011.07.029

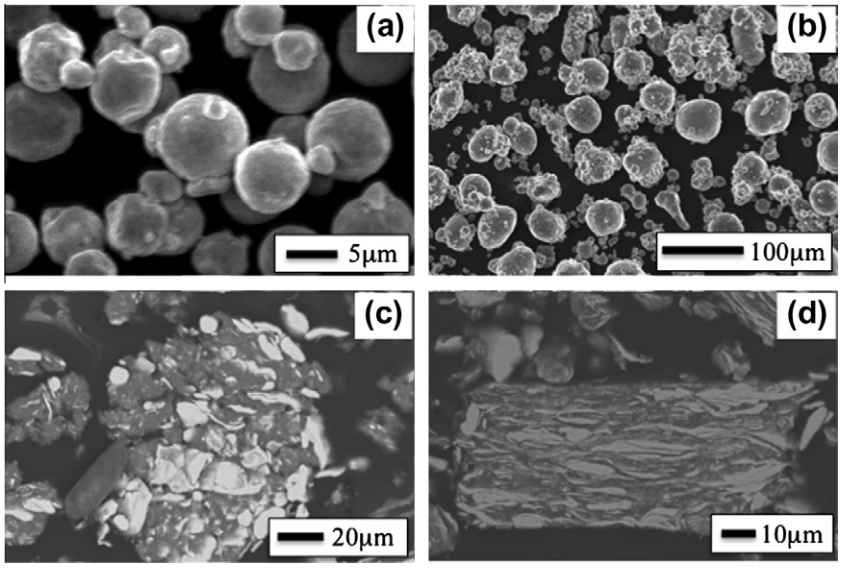

Fig. 3. Initial powder morphology and microstructural evolution of powders milled under ARM1 ball-milling conditions (see Tables 1 and 4). (a) 5–15 μm Ni powder. (b) H50 Al powder. (c) Unsieved ARM1 powder milled for 35% TTR (58 min). The milled particles have significant porosity and some of the Ni (light gray) particles are only slightly deformed. (d) Unsieved ARM1 powder milled for 65% TTR (108 min). The porosity observed in (c) is no longer visible and the Ni particles are heavily deformed.

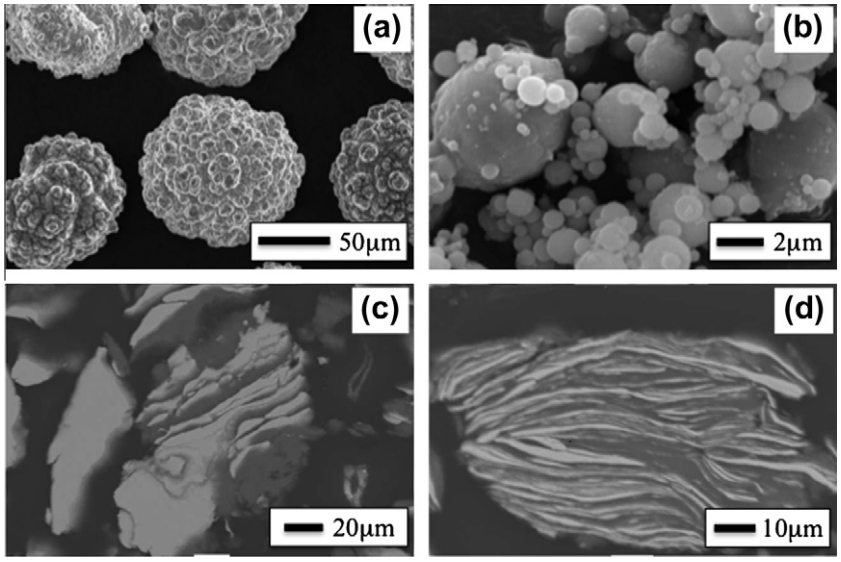

Fig. 4. Initial powder morphology and microstructural evolution of powders milled under ARM2 ball-milling conditions (see Tables 1 and 4). (a and b) 100 μm Ni particles and H2 Al particles, respectively. (c) Particle morphology for the powders milled for 74 min (35% TTR). The composite particles are flake-like without visible porosity. (d) Powder particles milled for 137 min (65% TTR). The laminate structure has been refined and the Ni is well dispersed throughout the particles.

ARM2 powders) is that the Ni layers (light gray) are much longer than in Fig. 4d. The same sized powders from Fig. 4 are used for powders milled with ARM3 conditions where the temperature is slightly higher, and the milling media is much smaller (i.e. lower mass). The evolution of the microstructure in this case is shown in Fig. 5. Powders milled for 35% TTR show a similar trend as in Fig. 4c where the Ni particles are elongated, but have a wavy appearance, which is attributed to the lower-energy impacts of the grinding media being unable to flatten completely the initially large Ni particles. The layered microstructure in Fig. 5b shows significant cracking with and across the direction of the layers. An important part of the ball-milling process is the fracture of particle grains, and the cracks shown here may indicate that impact conditions may be insufficient for complete particle fracture. At later milling times the composite Ni + Al particles appear to be blended much more in Fig. 5d, but Fig. 5a shows flattened Ni that are not bonded to any Al. In Fig. 5d the microstructure resembles that of a compaction process with small amounts of cold welding in comparison with Figs. 3 and 4 where a finely layered microstructure was observed for longer mill-

Please cite this article in press as: Herbold EB et al. Effects of processing and powder size on microstructure and reactivity in arrested reactive milled Al + Ni. Acta Mater (2011), doi:10.1016/j.actamat.2011.07.029

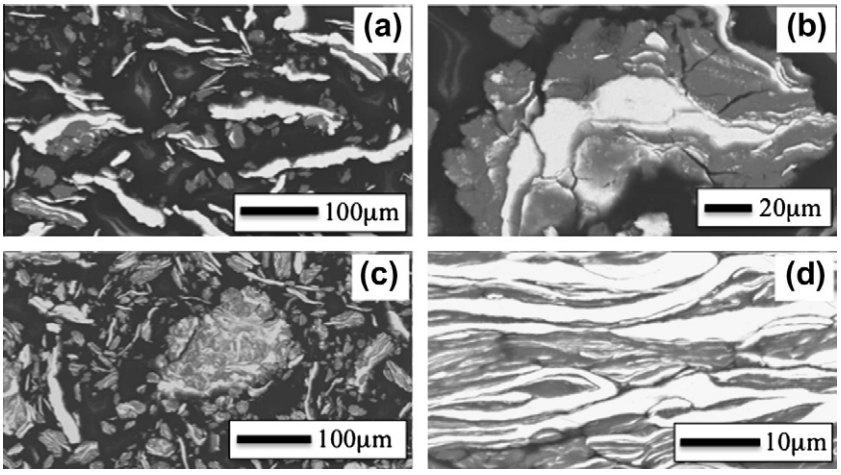

Fig. 5. Initial powder morphology and microstructural evolution of powders milled under ARM3 ball-milling conditions (see Tables 1 and 4). (a and b) Powder microstructure for powders milled for 71 min (35% TTR) with small (light) milling media. The initial powders are identical to (a) and (b) from Fig. 4. Cracks are clearly shown in larger particle agglomerates shown in (b) and the Ni powder is flattened into jagged rod or plate forms. (c and d) Powders milled for 132 min (65% TTR) showing further reduction of Ni particles. However, cracks and incomplete cold-welding is apparent in the large particle depicted in (d).

ing times. The particles milled with the smaller milling media may take longer to process into fine layered structures, but the weakly bonded layers are also signs that there may be a lower level of intermixing at the interface of the two layers. This point may be important for powders used for their energy output rather than the resultant intermetallic and is discussed in the thermal analysis [22].

3.3. Milling energy and time to reaction

The total energy of the impacts and the TTR are used to differentiate the data for the different milling conditions and powder sizes. An estimate for the total milling energy per gram of powder is [16,35]:

$$E^* = \frac{E_b n_b f_b t_r}{m_p}, \tag{1}$$

where E_b is the impact energy of a single collision, n_b is the number of balls, f_b is the frequency of impact, t_r is the measured TTR and m_p is the mass of the powder. In Ref. [36] the ball velocity within the vial generated by a Spex® 8000 high-energy ball-mill was found to depend on its size. Fig. 5 in Ref. [36] shows this relationship and an approximate expression for their experimental curve for ball sizes ranging from 5 to 10 mm is $v_b = 4.3-160d_b$, where the ball velocity v_b and ball diameter d_b have units of (m s^{-1}) and (m), respectively. An expression for the impact energy of a single ball is $E_b = 1/2\phi_b m_b v_b^2$, where ϕ_b is proposed in Ref. [35] as an efficiency factor related to the number of balls in the vial. Here, we use a similar approach where ϕ_b is the ratio of the volume of the media and powder to the volume of the empty vial,

$$\phi = 1 - \frac{m_b n_b}{V_v \rho_b} - \frac{m_p}{V_v \rho_{Ni_{0.5}Al_{0.5}}}, \tag{2}$$

where $V_v = 66\ \text{cm}^3$ is the volume of the vial, m_b, $\rho_b = 8\ \text{g cm}^{-3}$ and n_b are the mass of a single ball, the density and the number of balls, $\rho_{Ni_{0.5}Al_{0.5}} = 5.17\ \text{g cm}^{-3}$ for the $Ni_{0.5}Al_{0.5}$ powder, and m_p is the mass of the powder. In Ref. [37] the impact frequency was measured by an LVDT in a special ball-milling configuration containing only one ball for grinding media. However, since we are using multiple balls for each experiment an estimate for the frequency of impact of each ball is $f_b = 50\ \text{s}^{-1}$ since each ball must travel to one flat end of the vial and back each cycle and the period of oscillation of the vial is approximately 25 s^{-1}. Eqs. (1) and (2) may be evaluated from the data presented in Tables 1 and 2.

Fig. 6 shows the total energy (Eq. (1)) plotted as a function of the TTR scaled by the charge ratio $C_R = m_b/m_p$.

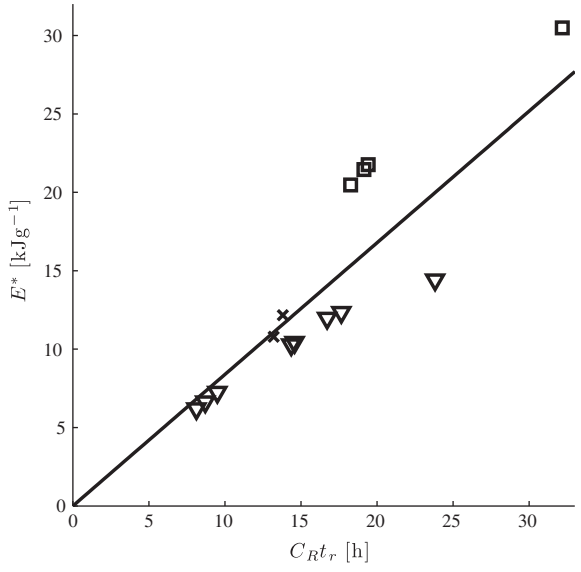

Fig. 6. The total energy plotted as a function of the time to reaction scaled by the charge ratio. The slope of the straight line is given by Eq. (3). The points above this line marked with □ are experiments with the 3.18 mm balls. The points marked with × and ▽ indicate that the 5.56 mm and 7.94 mm milling media were used.

The constant slope of the straight line, S, is taken from Eq. (1):

$$S = \frac{E_b n_b f_b}{C_R m_p} = \frac{f_b \phi_b v_b^2}{2}, \quad (3)$$

which is the relationship between the amount of free space within the vial and the velocity of the balls for a given frequency. The points above the straight line in Fig. 6 marked with □ are from experiments with the 3.18 mm balls. The points marked with × and ▽ indicate experiments where 5.56 and 7.94 mm milling media were used. The position of the points (□) above the line indicates that higher total impact energy is required for similar reaction times using small milling media. Points below the line indicate that less total impact energy is required for similar reaction times using large milling media. This result indicates that the use of larger milling media produces a higher defect density in contrast to the smaller, lighter balls. We observe that the TTR depends on the energy per impact separate from the total impact energy.

3.4. Analysis of variance (ANOVA) of the designed experiments

The TTR and the change in temperature due to the reaction were measured for each experiment in Table 1 and are listed in Table 2. There are seven variables present in the design of experiments and the analysis of variance separates the total variability into its component parts using Design Expert software [34]. Table 5 lists the component variability for two different linear statistical models that predict the TTR and the change in temperature during intermetallic formation. The final model for the TTR is:

$$t_r = -20000 d_b - 2000 r_{bp} + 700 m_p + 100 T_c + 70 d_{Al} + 1000000 m_{PCA}/m_p, \quad (4)$$

where t_r is the TTR (s), d_b (mm) is the diameter of the milling media, r_{bp} is the ball:powder ratio, m_p (g) is the mass of the powder, T_c (°C) is the control temperature, d_{Al} (μm) is the nominal size (diameter) of the Al powder and m_{PCA} (g) is the mass of the process control agent. The variation in size of the Ni powder was not statistically significant in this model and was not included in Eq. (4). Eq. (4) indicates that the diameter of the balls and the ball:powder ratio are the only two factors contributing to shorter milling times. This was also discussed in the previous section where the deviation of the data above or below Eq. (3) in Fig. 6 was related to the size of the milling media and indicated a dependence of single ball collision energy rather than sum total of impact energy through the ball-milling process. It is interesting that although the control temperatures were not varied greatly, with respect to cryogenic milling with liquid nitrogen, greater milling time is required for initiation of a self-sustained high-temperature synthesis of NiAl for higher vial wall temperatures.

The results shown in Fig. 2 were also used to derive a model that predicts the temperature change due to intermetallic formation:

Table 5
Analysis of variance (ANOVA) of the measured time to reaction (TTR) and the change in vial temperature due to intermetallic formation from Table 2 for the designed experiments (DOE) in Table 1. Column 3 gives the standard error of each term, in their respective units, in Eqs. (4) and (5). Columns 2 and 4–7 are given in terms of "coded" factors which scales the range of each variable from −1 to +1.

Source	Sum of squares	Std. error of term	Degrees of freedom	Mean square	*F*-value	*P*-value
TTR-Model	3.24×10^8		6	5.40×10^7	98.6	$<1.0 \times 10^{-4}$
Constant		±3000				
A – (d_b) ball diameter	2.51×10^7	±3000	1	2.51×10^7	45.9	3.0×10^{-4}
B – (r_{bp}) charge ratio	9.04×10^7	±200	1	9.04×10^7	165	$<1.0 \times 10^{-4}$
C – (m_p) powder mass	8.09×10^7	±60	1	8.09×10^7	148	$<1.0 \times 10^{-4}$
D – (T_c) temperature	6.32×10^6	±30	1	6.32×10^6	11.5	1.2×10^{-2}
E – (d_{Al}) Al size	1.94×10^7	±13	1	1.94×10^7	35.4	6.0×10^{-4}
G – (m_{PCA}/m_p)% PCA	2.80×10^7	±20,000	1	2.80×10^7	51.1	2.0×10^{-4}
Residual	3.84×10^6	–	7	5.48×10^5	–	–
Pure error	3.81×10^6	–	6	6.35×10^5	–	–
Total	3.28×10^8	–	13	–	–	–
Δ*T*-Model	740		7	106	63.4	$<1.0 \times 10^{-4}$
Constant		±2				
A – (d_b) ball diameter	27.2	±8	1	27.2	16.3	6.8×10^{-3}
B – (r_{bp}) charge ratio	9.82	±0.5	1	9.82	5.89	5.1×10^{-3}
C – (m_p) powder mass	65.7	±0.3	1	65.7	39.4	8.0×10^{-4}
D – (T_c) temperature	13.5	±0.05	1	13.5	8.10	2.9×10^{-3}
E – (d_{Al}) Al size	13.1	±0.05	1	13.1	7.83	3.1×10^{-3}
F – (d_{Ni}) Ni size	12.6	±0.01	1	12.6	7.54	3.4×10^{-3}
G – (m_{PCA}/m_p)% PCA	13.9	±30	1	13.9	8.36	2.8×10^{-3}
Pure error	10.0	–	6	1.67	–	–
Total	750	–	13	–	–	–

Please cite this article in press as: Herbold EB et al. Effects of processing and powder size on microstructure and reactivity in arrested reactive milled Al + Ni. Acta Mater (2011), doi:10.1016/j.actamat.2011.07.029

$$\Delta T = -17 + 34d_b + 1.2r_{\mathrm{bp}} + 1.8m_p + 0.15T_c - 0.16d_{\mathrm{Al}} - 0.04d_{\mathrm{Ni}} - 90m_{\mathrm{PCA}}/m_p. \quad (5)$$

It is interesting that, in contrast to Eq. (4), the initial size of the Ni particles is a significant factor in this model (see Table 5). Also, there is a dependence of the powder mass in three of the terms (r_{bp}, m_p, m_{PCA}/m_p) that balance one another, but the powder mass is the most significant factor in the expression. The diameter of the milling media (d_b), the particle sizes (d_{Al}, d_{Ni}) and the controlled temperature (T_c) contribute to the decrease in measured temperature during intermetallic formation. Eq. (5) indicates that the use of small Al particles are more important than small Ni particles with respect to greater thermal output. The standard error of each term in Eqs. (4) and (5) are given in Table 5 in their respective units.

3.5. Thermal analysis

Results from differential scanning calorimetry (DSC) are shown in Fig. 7 for ARM1–ARM3 powders milled for (a) 35% TTR and (b) 65% TTR. The first sign of intermetallic formation occurs at 240 and 220 °C for (a) and (b), respectively. This is probably due to the $NiAl_3$ reaction, which is known to be the first meta-stable intermetallic formed followed by Ni_2Al_3 then NiAl [10,23]. Is should be mentioned that there is no sign of the first major endothermic peak from stearic acid at 67 °C, which indicates that contamination from the PCA is not readily observed in thermal analysis [38].

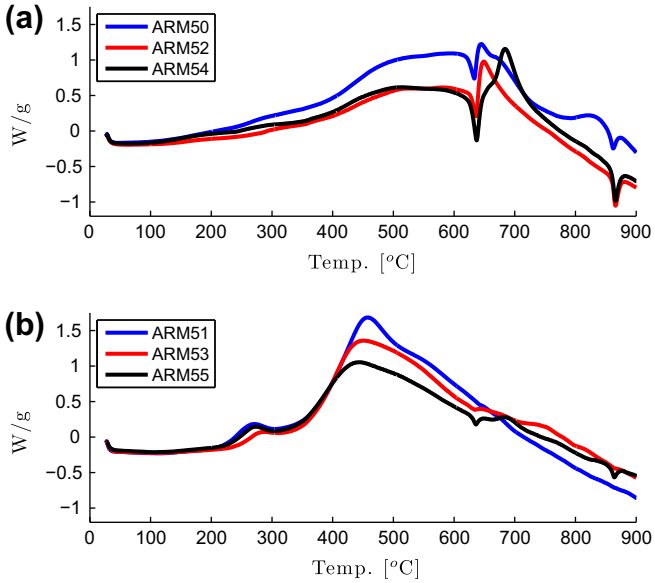

Fig. 7. DSC results for the milled powders. (a) Powders from Experiments 50, 51 and 52 using ARM1, ARM2 and ARM3 conditions are compared where each is milled for 35% TTR. The initiation temperature is not clearly defined, but is estimated to be between 400 and 450 °C. (b) Powders from Experiments 53, 54 and 55 using ARM1, ARM2 and ARM3 conditions are compared where each is milled for 65% TTR. Two distinct reactions are present, indicating the difference in reaction kinetics as a function of milling time for similar powders. All scans produced using a heating rate of 20 K min^{-1} with 110 ml min^{-1} Ar flow.

The powders with the highest thermal output per gram milled to 35% and 65% TTR are those prepared with ARM1 conditions (Experiments 50 and 53), which are shown in Fig. 3. In this case, the Al powder was much larger than for the ARM2 and ARM3 powders. However, the total milling time of the ARM1 powder is 20% less than the other two powders. It is possible that the milling time accounts for part of the discrepancy, but the small Al particles initially have 25 times more surface area coated with an oxide layer that is incorporated into the powder, which is another possibility.

The DSC curves for powders milled under ARM2 (Experiments 51 and 54) and ARM3 (Experiments 52 and 55) conditions are approximately the same at times corresponding to 35% TTR, but ARM3 releases less total energy than ARM2 in Fig. 7b. It was shown in Fig. 5d that the level of cold-welding was less significant than in Figs. 3 and 4 due to the size of the milling media. One possibility for the lower thermal output of ARM3 in Fig. 7b is that there is poor mechanical/thermal contact at the interface of the particles (see Fig. 5d), which requires more energy to complete the reaction. Despite the differences between the magnitudes of the DSC data, the initiation temperatures of the reactions are quite similar between these powders milled under three different conditions. This suggests that similar reaction initiation responses can be expected from thermal analysis for powders milled to similar TTR percentages.

3.6. X-ray diffraction results

Fig. 8 compares powder XRD measurements for six powders milled under ARM1–ARM3 conditions and one from Experiment 29 (reacted) shown at the bottom of each subfigure. In Fig. 8a the top three scans are from powders listed in Table 4 as Experiments 57 (blue), 59 (red) and 61 (black), corresponding to ARM1–ARM3 conditions milled to 35% TTR. The middle three scans are from Experiments 58 (blue), 60 (red) and 62 (black), corresponding to ARM1–ARM3 conditions milled to 65% TTR. There is negligible alloy formation for the data corresponding to milling times of 35% and 65% TTR and the scan for the reacted powder (i.e. Experiment 29) shows that the powder is composed almost entirely of NiAl. This was observed in Refs. [4,16] where it is reported that continuous milling may produce alloying at the grain scale, but self-propagating reactions indicated by post-mortem appearance of nickel aluminides in XRD scans were very sudden. However, increased milling time broadened and decreased the height of the individual Ni and Al peaks. In Ref. [39], XRD peak aberrations are attributed to various sources of strain. Comparing the powders milled for 35% TTR, the full-width-half-maximum values for ARM1 are greater than for ARM2 or ARM3 powders at almost every major peak. This indicates either a higher dislocation density or smaller crystallite size, but may also be characteristic of the starting powders (i.e. small Ni particles). Comparing

Please cite this article in press as: Herbold EB et al. Effects of processing and powder size on microstructure and reactivity in arrested reactive milled Al + Ni. Acta Mater (2011), doi:10.1016/j.actamat.2011.07.029

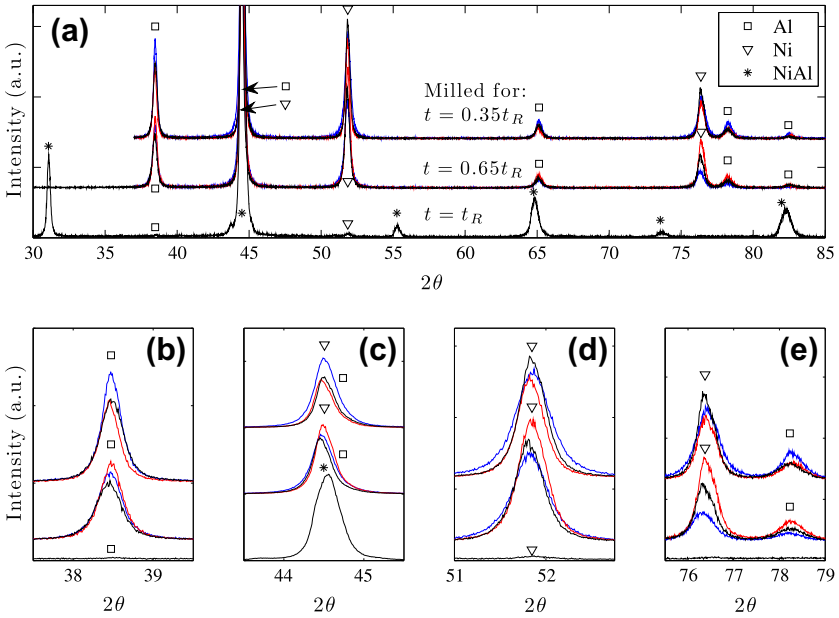

Fig. 8. XRD scans for six powders milled under ARM1–ARM3 conditions and one from Experiment 29 (reacted) shown at the bottom of each subfigure. (a) The top three scans are from powders listed in Table 4 as Experiments 57 (blue), 59 (red) and 61 (black), corresponding to ARM1–ARM3 conditions milled to 35% TTR. The middle three scans are from Experiments 58 (blue), 60 (red) and 62 (black), corresponding to ARM1–ARM3 conditions milled to 65% TTR. The top, middle and bottom scans are shifted arbitrarily for comparison. (b)–(e) The same seven scans are plotted and shifted vertically to highlight the difference in four different Bragg peaks. The □, ▽ and ∗ indicate the presence of Al, Ni and NiAl, respectively. (For interpretation of the references to colour in this figure legend, the reader is referred to the web version of this article.)

the powders milled for 65% TTR, the peak widths are approximately equal for $2\theta = 37$–$54°$, but a slight difference in asymmetric peak broadening indicates different levels of dislocations, stacking faults, twinning and crystallite size. An investigation of the effects of ball-milling NiAl powder powders beyond SHS can be found in Ref. [21].

4. Discussion

The DSC data shows a dependence of the thermal performance on microstructure. In applications where ARM materials are being produced for potential chemical energy sources with rapid heat production, the rate of reaction and

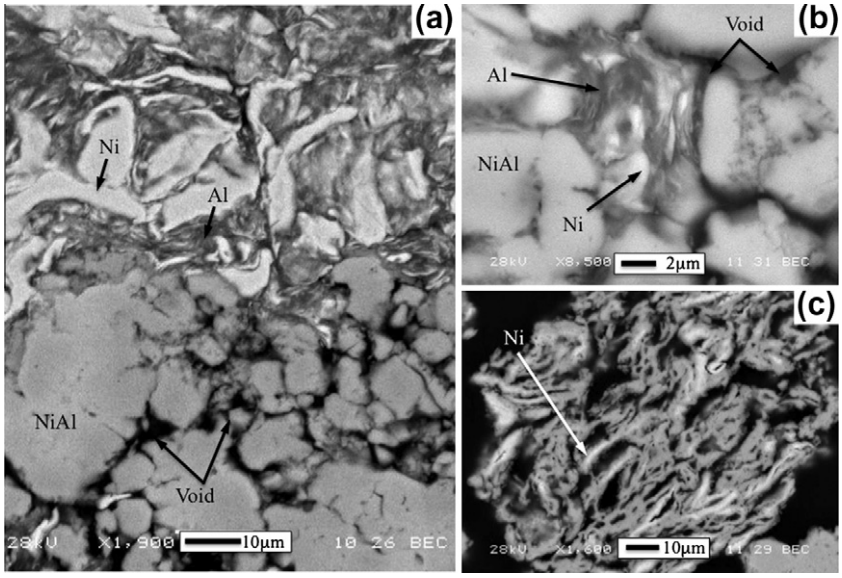

Fig. 9. BEC image of partially reacted powder agglomerate for Experiment 29. (a) The bottom portion is NiAl, the darker gray is Al and the light gray is Ni. The NiAl is shown as small separated grains at the bottom of the figure. The reaction propagation moved from the bottom to the top of the image before being arrested. (b) A small amount of powder is completely surrounded by intermetallic NiAl. The reaction stopped along the right side through the separate surfaces, but the propagating reaction ceased during reaction on the left. (c) Arrested reaction within a particle where there is a clear concentration gradient from Ni to NiAl.

Please cite this article in press as: Herbold EB et al. Effects of processing and powder size on microstructure and reactivity in arrested reactive milled Al + Ni. Acta Mater (2011), doi:10.1016/j.actamat.2011.07.029

total energy output are more important than the resulting intermetallic. This means that the processing conditions must balance the size and size distribution of the layered microstructure, the interfacial mixing between components (see Figs. 3–5) as well as the defect density in the constituent materials if the reaction of the powders are to be mechanically initiated. Additionally, the process of particle size reduction by high-energy ball-milling is capable of producing layer thickness on the order of tens of nanometers, while the particle sizes may be on the order of 10–100 μm. This reduces the need to initially use ultrafine particles for further reduction since the oxide layer may be considered a non-negligible contaminant for particles that are sufficiently small.

Fig. 9 shows three instances of partially reacted particles from Experiment 29. The compositions indicated in this figure were identified by the EDS at different points within the image. The arrows pointing to NiAl correspond to places where there is a 1:1 ratio of Ni and Al by atomic percentage. In addition to the composition provided by the EDS, Fig. 8 shows that the powder from Experiment 29 is composed almost entirely of NiAl. The arrows point to singular compositions of Ni and Al, which had the lightest and darkest gray tones, respectively. The NiAl color corresponds to a gray tone between Ni and Al. These three examples typify the occurrence of partially reacted particles observed in the other reacted powders (see Fig. 2). In Fig. 9a an intermetallic reaction has occurred, producing NiAl (at the bottom) and consuming layered material ahead of the SHS reaction. It is interesting that there is no visible barrier indicating the cause of the arrested reaction. For example, the reaction did not simply reach a crack in the particle or a band of Ni or Al. Void space is visible in the bottom of Fig. 9a, on the right side of Fig. 9b and throughout the particle shown in Fig. 9c. This volume contraction is due to the difference in density between mixed Ni + Al (5.17 g cm^{-3}) and the compound NiAl (5.85 g cm^{-3}) [4,40,41]. In Fig. 9a this void space on the bottom half of the figure indicates the reaction has ceased despite the appearance of thermal contact between the NiAl formations and unreacted material. Fig. 9b shows unreacted material that is completely surrounded by NiAl. On the left side of the unreacted material the spatial gradation of grayscale tone corresponds to compositional differences from NiAl to Al or Ni and there is a clear separation of material on the right side of the unreacted portion. Both Fig. 9a and b shows arrested reaction within grains where the reaction likely ceased due to the insufficient heating of the unreacted material by NiAl.

Fig. 9c shows an arrested reaction where the particle has excess Ni. Ni-rich bands are shown adjacent to NiAl where the grayscale indicates concentration gradients. While Ni-rich compounds have been synthesized by ball-milling, this particular particle may require further reduction in crystallite size for the subsequent reaction to occur [9].

The details shown by Fig. 9 elucidate the processes occurring during explosive reaction within ball-milled particles. The partially reacted grains suggest that the composite particles are forming an intermetallic between layers within the particle and not at the grain scale.

5. Conclusions

The measured TTR and change in temperature during SHS of NiAl were investigated with powders composed of equiatomic Ni + Al of different sizes processed under different milling conditions specified by statistically designed experiments. Ball-milling conditions and powder particle sizes of Al + Ni powders were varied and linear statistical models predicting the TTR and the change in temperature (ΔT) were found. The times required to observe SHS with different combinations of the powders and ball-milling conditions vary by almost an order of magnitude. The TTR depends on the energy per impact as distinct from the total impact energy. Comparisons of powders milled to times corresponding to percentages of their averaged TTR show similar reaction initiation temperatures despite the difference in total milling time. Several distinct arrested reactions within the powder grains show explosive reactions with rapid solidification or incomplete diffusion of Ni into Al, forming porous, partially reacted, Ni-rich layered structures. The partially reacted grains suggest that the composite laminate particles are not forming intermetallic on the grain scale, but on the localized scale between layers.

Acknowledgements

E.B.H. would like to thank the Florida Institute for Research in Energetics (FIRE) for support and J.M. Scott for adding the temperature control capability to the ball mill. E.B.H. would also like to thank R. Huffman and D.W. Richards for assistance with the DSC and XRD scans. Funding for this research was provided by the University of Florida through the task order 9-0015 from AFRL at Eglin AFB, Contract No. FA8651-08-D-0108.

References

[1] Benjamin JS. Metall Trans 1970;1:2943.
[2] Gilman PS, Benjamin JS. Annu Rev Mater Sci 1983;13:279.
[3] Ivanov E, Grigorieva T, Golubkova G, Boldyrev V, Fasman AB, Mikhailenko SD, et al. Mat Lett 1988;7:51.
[4] Atzmon M. Phys Rev Lett 1990;64:487.
[5] Suryanarayana C, Froes FH. Adv Mater 1993;5:93.
[6] Cardellini F, Mazzone G, Vittori Antisari M. Acta Mater 1996;4:1511.
[7] Koch CC. NanoStruct Mat 1997;9:13.
[8] Thadhani NN. Mechanochemical synthesis of intermetallic compounds. In: Westbrook JH, Fleischer RL, editors. Intermetallic compounds: principles and practice. New York: John; 2002.
[9] Portnoy VK, Blinov AM, Tomilin IA, Kusnetsov VN, Kulik T. J Alloys Comp 2002;336:196.
[10] Zhu HX, Abbaschian R. J Mat Sci 2003;38:3861.
[11] Schoenitz M, Ward T, Dreizin EL. Mater Res Soc Symp Proc 2004;800:AA2.6.1.
[12] Moshksar MM, Mirzaee M. Intermetallics 2004;12:1361.

[13] Umbrajkar SM, Schoenitz M, Dreizin EL. Propellants Explos Pyrotech 2006;31:382.
[14] Umbrajkar SM, Schoenitz M, Dreizen EL. J Alloys Comp 2005;402:70.
[15] Morsi K, Shinde S, Olevsky EA. J Mater Sci 2006;41:5699.
[16] Joardar J, Pabi SK, Murty BS. J Alloys Comp 2007;429:204.
[17] Shteinberg AS, Knyazik VA. Pure Appl Chem 1992;64:965.
[18] Herbold EB, Thadhani NN, Jordan JL. J Appl Phys 2011;109:066108.
[19] Dunbar E, Thadhani NN, Graham RA. J Mat Sci 1993;28:2903.
[20] Boslough MB. Chem Phys Lett 1989;160:618.
[21] Chen T, Hampikian JM, Thadhani NN. Acta Mater 1999;47:2567.
[22] Mann AB, Gavens AJ, Reiss ME, Van Heerden D, Bao G, Weihs TP. J Appl Phys 1997;82:1178.
[23] Colgan EG, Nastasi M, Mayer JW. J Appl Phys 1985;58:4125.
[24] Shteinberg AS, Lin Y-C, Son SF, Mukasyan AS. J Phys Chem 2010;114:6111.
[25] Mukasyan AS, White JDE, Kovalev DY, Kochetov NA, Ponomarev VI, Son SF. Physica B 2010;405:778.
[26] Zhao S, Germann TC, Strachan A. J Chem Phys 2006;125:164707.
[27] Suryanarayana C. Mechanical alloying and milling. Boca Raton, FL: CRC Press; 2004.
[28] Eakins DE, Thadhani NN. Int Mat Rev 2009;54:181.
[29] Crone JC, Knap J, Chung PW, Rice BM. Proceedings of the 14th symposium (international) on detonation; 2010. ID#30026.
[30] Armstrong RW, Baschung B, Booth DW, Samirant M. Nano Lett 2003;3:253.
[31] Reeves RV, White JDE, Mukasyan AM, Son SF. Proceedings of the American physical society topical group on shock compression of condensed matter. AIP conference proceedings, vol. 1195; 2009. p. 466–9.
[32] DeCastro CL, Mitchell BS. Nanoparticles from mechanical attrition. In: Baraton M-I, editor. Synthesis, functionalization and surface treatment of nanoparticles. Valencia, CA: American Scientific Publishers; 2002.
[33] Montgomery DC. Design and analysis of experiments. 5th ed. New York: John Wiley; 2001.
[34] http://www.statease.com/dx8descr.html.
[35] Murty BS, Mohan Rao M, Ranganathan S. Acta Metall Mater 1995;43:2443.
[36] Bassett D, Matteazzi P, Miani P. Mat Sci Eng 1994;A174:71.
[37] Chen Y, Bibole M, Le Hazif R, Martin G. Phys Rev B 1993;48:14.
[38] Jaw KS, Hsu CK, Lee JS. Thermo Acta 2001;367–368:165.
[39] Ungar T. Scripta Mat 2004;51:777.
[40] Villars P, Calvert D. Pearson's handbook of crystallographic data for intermetallic phases, vol. II. Metals Park, OH: American Society for Metals; 1985. p. 1038.
[41] Miracle DB. Acta Metall Mater 1993;41:649.

Please cite this article in press as: Herbold EB et al. Effects of processing and powder size on microstructure and reactivity in arrested reactive milled Al + Ni. Acta Mater (2011), doi:10.1016/j.actamat.2011.07.029

DISTRIBUTION LIST
AFRL-RW-EG-TP-2012-002

*Defense Technical Info Center
8725 John J. Kingman Rd Ste 0944
Fort Belvoir VA 22060-6218

AFRL/RWME (6)
AFRL/RWOC-1 (STINFO Office)